

Communication

# Waste-Coffee-Derived Activated Carbon as Efficient Adsorbent for Water Treatment

Hong-Ming Chen <sup>1,2</sup>, Woon-Ming Lau <sup>1,2</sup> and Dan Zhou <sup>1,2,\*</sup>

<sup>1</sup> Beijing Advanced Innovation Center for Materials Genome Engineering & Center for Green Innovation, School of Mathematics and Physics, University of Science and Technology Beijing, Beijing 100083, China  
<sup>2</sup> Shunde Innovation School, University of Science and Technology Beijing, Foshan 528000, China  
\* Correspondence: zhoudan@ustb.edu.cn

**Abstract:** Activated carbon prepared from waste coffee was utilized as a potential low-cost adsorbent to remove Rhodamine B from aqueous solution. A series of physical characterizations verify that the obtained activated carbon possesses a layered and ordered hexagonal structure with a wrinkled and rough surface. In addition, high specific surface area, appropriate pore distribution, and desired surface functional groups are revealed, which promote the adsorption properties. Various adsorption experiments were conducted to investigate the effect on the adsorption capacity (e.g., of initial dye concentration, temperature and solution pH) of the material. The results showed that the waste-coffee-derived activated carbon with a large surface area of approximately  $952.7 \text{ m}^2 \text{ g}^{-1}$  showed a maximum uptake capacity of  $83.4 \text{ mg g}^{-1}$  at the pH of 7 with the initial dye concentration of  $100 \text{ mg L}^{-1}$  under  $50^\circ\text{C}$ . The higher adsorption capacity can be attributed to the strong electrostatic attraction between the negatively charged functional groups in activated carbon and the positively charged functional groups in RB. The kinetic data and the corresponding kinetic parameters were simulated to evaluate the mechanism of the adsorption process, which can fit well with the highest  $R^2$ . The adsorption results confirmed the promising potential of the as-prepared waste-coffee-derived activated carbon as a dye adsorbent.



**Citation:** Chen, H.-M.; Lau, W.-M.; Zhou, D. Waste-Coffee-Derived Activated Carbon as Efficient Adsorbent for Water Treatment. *Materials* **2022**, *15*, 8684. <https://doi.org/10.3390/ma15238684>

Academic Editors: Farooq Sher and Roberta G. Toro

Received: 9 November 2022

Accepted: 1 December 2022

Published: 6 December 2022

**Publisher's Note:** MDPI stays neutral with regard to jurisdictional claims in published maps and institutional affiliations.



**Copyright:** © 2022 by the authors. Licensee MDPI, Basel, Switzerland. This article is an open access article distributed under the terms and conditions of the Creative Commons Attribution (CC BY) license (<https://creativecommons.org/licenses/by/4.0/>).

**Keywords:** rhodamine B; adsorption; waste coffee; activated carbon; surface properties

## 1. Introduction

With the development of human society, the pursuit of a good environment and good health becomes more and more important. However, due to inefficient past development, environmental pollution can be seen everywhere on Earth, which severely harms humans. For example, various dyes are widely used in many industries, such as clothing, food, papermaking, cosmetics, biological stains and plastics [1–6]. Although these dyes have some desired benefits, they can be accompanied by many problems. Specifically, Rhodamine B (RB) is one of the most important dyes. It has been widely used as a fluorescent dye agent in the laboratory, in stained glass, in special fireworks and in other industries [7–9]. However, RB is also reported to be deleterious and carcinogenic for human beings and animals [10,11]. Moreover, it is usually stable in the environment and non-biodegradable [12]. Therefore, the removal of RB from waste water is very important for the protection of aquatic life, the environment and public health.

Many approaches have been reported for the removal of RB from waste water, such as photocatalytic degradation [13–18], liquid–liquid extraction through membrane technology [19], the electro-Fenton process [20], electrochemical oxidation [21], biodegradation [22] and microwave- or ultrasonic-assisted methods [7]. Among these, the photocatalytic degradation method has received wide attention. With this method, chemically complex organic pollutants might degrade into simpler, non-polluting molecules. However, these resultant products might not be good for wildlife because they still exist in waste water. The most direct and effective way is to remove the organic pollutants from waste

by adsorption. This method is currently attracting substantial attention [23,24]. Activated carbon has shown extreme potential for dye adsorption due to its porous structure, remarkably large surface area, and in turn high adsorption properties [25]. However, due to the high cost, the application for removing dyes in industry is still limited. Thus, the synthesis of low-cost activated carbons is greatly desired.

Coffee is one of the most popular drinks in the world, and hundreds of millions of bags of coffee are consumed every year [26]. Most of the waste coffee is treated as garbage for disposal. It will undoubtedly be an economical matter if coffee waste is used as raw material to produce activated carbon. Therefore, the exploration of an effective design and synthesis route from waste coffee to activated carbon seems to be significantly valuable. Herein, we report a simple method to prepare activated carbon with waste coffee as the starting material, aiming to propose a simple and low-cost method to produce activated carbon and simultaneously solve the recovery and utilization of waste coffee. The porous structure of the as-prepared activated carbon is characterized in detail, and then its application in removing RB from aqueous solution is investigated. This paper aims to combine the recycling of waste coffee with sewage treatment to reduce environmental pollution.

## 2. Materials and Methods

### 2.1. Activated Carbon Synthesis

Waste-coffee-derived activated carbon was prepared by a simple method. The first step involved carbonization, in which the waste coffee (4.0 g) was dried at 80 °C for 10 h and then annealed at 900 °C for 1 h in argon with a heating rate of 5 °C min<sup>-1</sup>. The second step was pore forming, in which the above as-prepared sample (2.0 g) and KOH (2.0 g) were dispersed in 20 mL deionized water and then heated at 65 °C for 16 h under stirring. The mixed solution was then dried at 100 °C for 20 h, and the remaining solid product was annealed at 900 °C for 1 h in argon. Finally, the sample was washed with 2 M hydrochloric acid and then with deionized water until the pH value was 7. The activated carbon was obtained after the subsequent filtration and drying process.

### 2.2. Materials Characterization

The surface morphologies of the as-prepared samples were obtained using scanning electron microscopy (SEM, Hitachi S-5200). The crystal structure of the samples was studied by X-ray diffraction (XRD, D/max 2200/PC) using Cu K $\alpha$  radiation with  $\lambda = 1.5046 \text{ \AA}$ . The specific surface area and pore features were investigated by means of nitrogen adsorption/desorption isotherms with an Autosorb-iQ system. The surface chemical state of the samples was analyzed by employing X-ray photoelectron spectroscopy (XPS, ESCALAB 250Xi). The functional groups of samples were obtained using Fourier transform infrared (FTIR, Nicolet iS50). Thermogravimetric analysis (TGA) (TG 8121 Rigaku Corp) was used at a heating rate of 10 °C min<sup>-1</sup> in nitrogen flow.

### 2.3. Adsorption Experiments

Adsorption experiments were carried out using activated carbon prepared by waste coffee as the adsorbent. RB was used as the adsorbate to prepare a stock solution of concentration of 20.9 mmol L<sup>-1</sup> (10 g L<sup>-1</sup>). This solution was used to prepare the required testing samples with the concentration of 208.7 to 626  $\mu\text{mol L}^{-1}$  (100 to 300 mg L<sup>-1</sup>). RB adsorption experiments were conducted in 500 mL glass flasks. A 200 mL RB aqueous solution containing 0.2 g activated carbon was poured into a glass flask. After that, the glass flask was covered and placed in a magnetic stirrer at 100 rpm and 50 °C. The concentration of the mixture solution was then determined at defined intervals of time using an ultraviolet visible spectrophotometer (LAMBDA 950). The maximum absorbance of RB was shown at a wavelength of 553 nm. A calibration curve was carried out for a series of RB solutions with specified concentrations, and the residual RB concentration of solution was obtained using the calibration curve. Amounts of 1 M HCl and 0.1 M KOH were used to adjust the pH of the RB solution.

The series of values were fitted using Langmuir and Freundlich isotherm models, which are shown with the equations [23,24,27] below:

$$\text{Langmuir : } \frac{C_e}{Q_e} = \frac{1}{Q_m K_L} + \frac{1}{Q_m} C_e \quad (1)$$

$$\text{Freundlich : } \log Q_e = \log K_F + \frac{1}{n} \log C_e \quad (2)$$

where  $Q_m$  ( $\text{mg g}^{-1}$ ) refers to the maximum adsorption capacity of RhB;  $K_L$  ( $\text{L mg}^{-1}$ ) represents the Langmuir adsorption constant that is associated with the adsorption affinity; and  $K_F$  ( $(\text{mg g}^{-1}) (\text{L g}^{-1})^{1/n}$ ) and  $n$  correspond to the Freundlich constants.

Pseudo-first-order and pseudo-second-order kinetic models are employed to investigate the isotherm kinetic, as revealed in the equations [27] below:

$$\text{Pseudo - first order : } \ln(Q_e - Q_t) = \ln Q_e - K_1 t \quad (3)$$

$$\text{Pseudo - second order : } \frac{t}{Q_t} = \frac{1}{K_2 Q_e^2} + \frac{1}{Q_e} t \quad (4)$$

where  $Q_e$  ( $\text{mg g}^{-1}$ ) and  $Q_t$  ( $\text{mg g}^{-1}$ ) correspond to the amount of RB adsorbed in activated carbon at equilibrium and at time  $t$ , respectively;  $t$  (min) refers to the contact time; and  $K_1$  and  $K_2$  represent the rate constants of pseudo-first order and pseudo-second order, respectively.

### 3. Results and Discussion

#### 3.1. Physical Properties of The Activated Carbon

SEM and EDS measurements were used to examine the morphology, microstructure and element composition of the as-prepared activated carbon. From the SEM images (Figure 1a–d) of the different scales, it can be seen that the sample exhibits a slightly wrinkled and rough surface. The special structure can help to improve the surface area of activated carbon. Figure 1e–h show that the as-prepared activated carbon contains three elements of carbon, oxygen and nitrogen, indicating that the functional groups containing oxygen and nitrogen exist on the surface of the activated carbon.

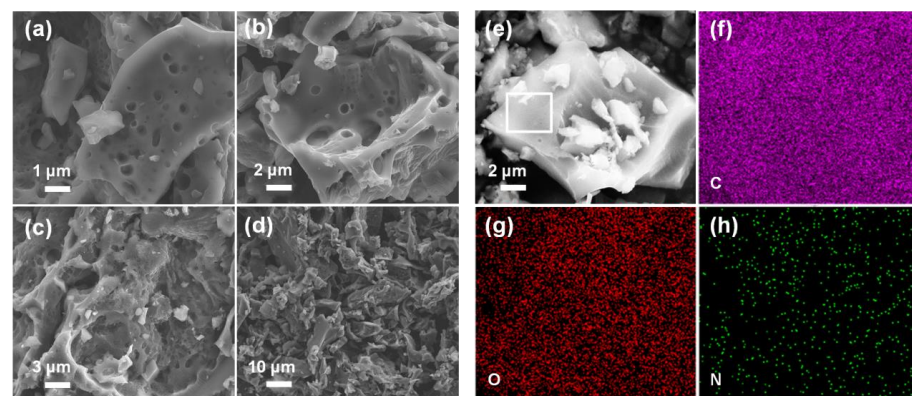


**Figure 1.** (a–d) SEM images of the activated carbon with different scales. (e–h) SEM images and EDS elemental maps of the activated carbon.

Figure 2a shows the XRD pattern of the activated carbon. It is obvious that the XRD pattern exhibits two broad peaks of (002) at  $22.3^\circ$  and (100) at  $42.9^\circ$ , which are assigned to the layered carbon and ordered hexagonal carbon, respectively [28]. The nitrogen adsorption–desorption isotherms and the corresponding pore size distribution of the sample were calculated by the Barrett–Joyner–Halenda (BJH) method, and the results are shown in Figure 2b. It indicates a type-I isotherm, which is a typical characteristic of

microporous material conforming to the pore size distribution, and the surface area of the sample is about  $952.7 \text{ m}^2 \text{ g}^{-1}$ . This unique porous feature contributes to the improvement of the adsorption properties of the activated carbon.

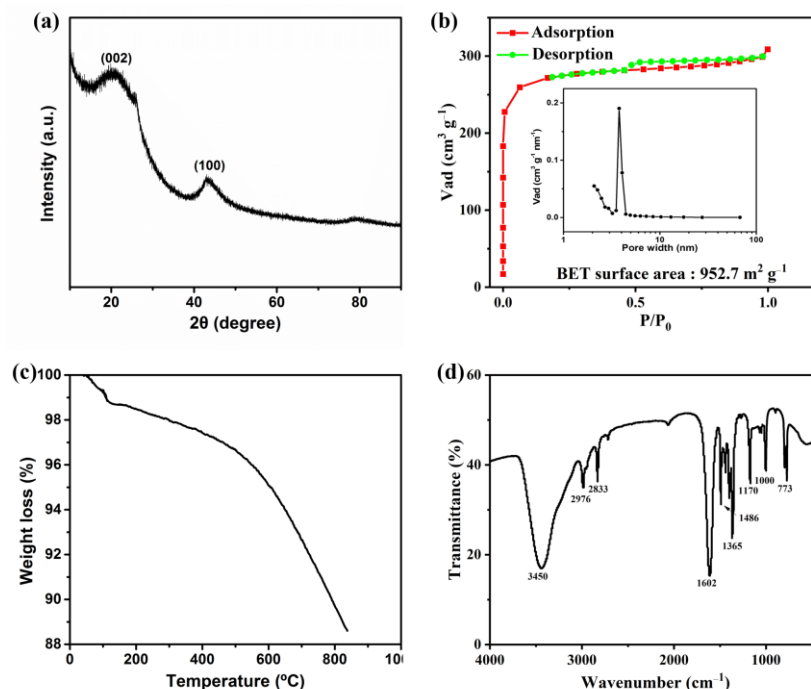


**Figure 2.** (a) XRD pattern of the activated carbon. (b) Nitrogen adsorption–desorption curves and pore size distribution of the activated carbon. (c) TGA and (d) FTIR spectra of the activated carbon.

Figure 2c shows the thermogravimetric (TG) curves of the activated carbon prepared from waste coffee in a nitrogen flow. The thermogravimetric curves of the activated carbon consist of two main stages of dehydration and pyrolysis. The reduction in the weight of activated carbon in the range of  $50\text{--}100 \text{ }^\circ\text{C}$  is due to the evaporation of adsorbed water. In the range of  $500\text{--}900 \text{ }^\circ\text{C}$ , a large weight loss occurred, which should come from the decomposition of the surface functional groups of the activated carbon [29]. Figure 2d shows the FTIR spectrum of activated carbon. The broad peak at  $3450 \text{ cm}^{-1}$  is attributed to the stretching O–H bond in hydroxyl groups or NH stretch, while the peak located at  $(1640 \text{ to } 1560) \text{ cm}^{-1}$  shows the asymmetric stretching of the carboxylate ( $-\text{COO}-$ ) group [10]. The peaks at  $2976$  and  $2833 \text{ cm}^{-1}$  may be attributed to the presence of C–H stretch, and the peak at  $1480 \text{ cm}^{-1}$  indicates the C=C bonds. The FTIR spectrum of the activated carbon shows major peaks at  $1365$ ,  $1170$ ,  $1000$  and  $773 \text{ cm}^{-1}$ , which correspond to the presence of C–C bonds, C–O stretching vibration, C–N stretching and C–H bonds [30–32].

To further confirm the surface functional groups on the as-prepared activated carbon, XPS analysis was investigated. Figure 3 shows the C 1s (a), O 1s (b), N 1s (c) and XPS survey spectra (d) of the activated carbon. The C 1s spectrum of the activated carbon usually consists of three types of carbon bonds: C–C or C=C ( $284.8 \text{ eV}$ ), C–O ( $286 \text{ eV}$ ) and O–C=O ( $289 \text{ eV}$ ) [29–34]. The O 1s peaks could be fitted to three curves: C=O at  $531.2 \text{ eV}$ , O–H or C–O–C at  $533 \text{ eV}$  and O–C=O at  $535.3 \text{ eV}$  [32]. The contents of carbon, oxygen and nitrogen on the surface of the carbon material were also obtained, which were  $79.7$ ,  $18.2$  and  $2.1\%$ , respectively. In addition, the content of carboxyl on the surface of the activated carbon was  $19.4\%$ . The carboxyl and hydroxyl groups could dissociate and then be negatively charged [35]. They could then be active sites in the adsorption process.

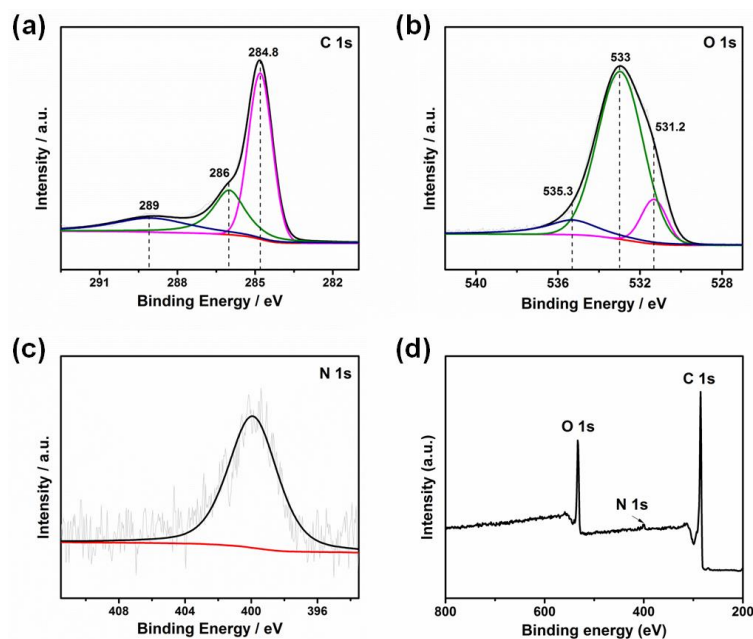


**Figure 3.** (a) C 1s, (b) O 1s, (c) N 1s and (d) survey XPS spectra of activated carbon.

### 3.2. Adsorption Properties Investigation

#### 3.2.1. The Effect of Initial RB Concentration

Figure 4 shows the effect of initial RB concentration on adsorption efficiency. These results revealed that in the first 3 h, the amount of RB adsorbed increased rapidly, and the adsorption on activated carbon no longer changed significantly after 6 h. Therefore, the corresponding time could be considered as the equilibrium time. The adsorb ability of the activated carbon to RB is increased by only  $3.3 \text{ mg g}^{-1}$ , with the initial concentration of RB increasing from  $100 \text{ mg L}^{-1}$  to  $300 \text{ mg L}^{-1}$ . This result indicated that a further increase in the concentration of RB does not affect the uptake capacity significantly due to the saturation of the adsorption sites [36].

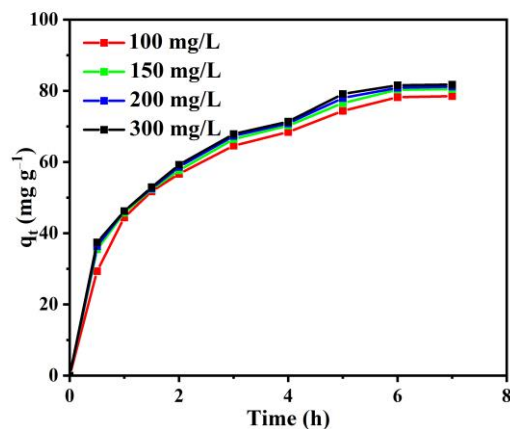


**Figure 4.** Effect of initial RB concentration on RB removal efficiency at  $\text{pH} = 5$  and  $T = 50 \text{ }^\circ\text{C}$ .

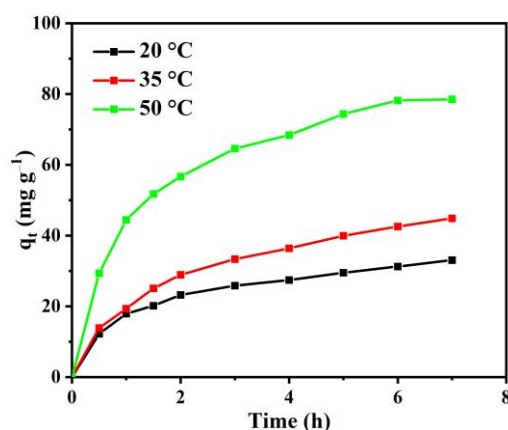
Adsorption isotherm models of Langmuir and Freundlich models were applied to evaluate the performance of the as-prepared activated carbon on the removal of RB from aqueous solution, and the corresponding parameters are shown in Table 1 (Equations (1) and (2)). For all of the isotherm models, the Langmuir model presents the results better than the Freundlich model with a higher  $R^2$ , suggesting a monolayer process for the activated carbon toward the adsorption of RB [37].

**Table 1.** Adsorption isotherm constants for RB adsorption onto the activated carbon (Equations (1) and (2)).

Sample	Isotherm Models					
	Langmuir			Freundlich		
	$Q_m$ ( $\text{mg g}^{-1}$ )	$K_L$ ( $\text{L mg}^{-1}$ )	$R^2$	$K_F$ ( $\text{mg g}^{-1}$ ) ( $\text{L/mg}^{1/n}$ )	$1/n$	$R^2$
Activated Carbon	83.3	0.86	0.999	74.3	0.018	0.975

### 3.2.2. The Effect of Temperature

In order to research the effect of solution temperature on the uptake capacity of the activated carbon, a bath experiment with different temperatures was carried out. The results are shown in Figure 5. Obviously, the amount of RB adsorbed per unit mass of the activated carbon increased with the temperature from 20 to 50 °C, indicating that the uptake capacity of the activated carbon depends on temperature significantly.

**Figure 5.** The effect of temperature on uptake capacity of activated carbon at an initial RB concentration of  $100 \text{ mg L}^{-1}$  and  $\text{pH} = 5$ .

As analyzed above, the obtained activated carbon displays a microporous feature, and the unique pore size distribution can lead to an increase in the adsorption capacity with increases in temperature. The molecular size of RB is nearly 2 nm. Therefore, after the pore has been adsorbed by the RB molecule at the entrance, it will impede the subsequent adsorption of RB molecules. The diffusion rate of RB molecules into the pores will be enhanced with increasing temperatures due to the endothermic diffusion process [38]. Therefore, the uptake capacity of the activated carbon improved to some extent as the temperature increased.

### 3.2.3. The Effect of Solution PH

To investigate the effect of solution pH on the uptake capacity of the activated carbon, a series of adsorption experiments with a different pH (from 3 to 11) were carried out, where the initial RB concentration was  $100 \text{ mg L}^{-1}$  and the temperature was 50 °C. The obtained results are shown in Figure 6, and demonstrate that the uptake capacity of the activated carbon was changed as the pH increased from 3 to 11. The maximum value of the adsorption capacity occurred at pH 7, which was  $83.4 \text{ mg g}^{-1}$ . Compared with some reported materials (e.g., ZIF-8, ZIF-67, ZIF-8@ZIF-67 [39]; polyamide grafted carbon microspheres [40]), the adsorption capacity of the activated carbon delivers a relatively desirable level.

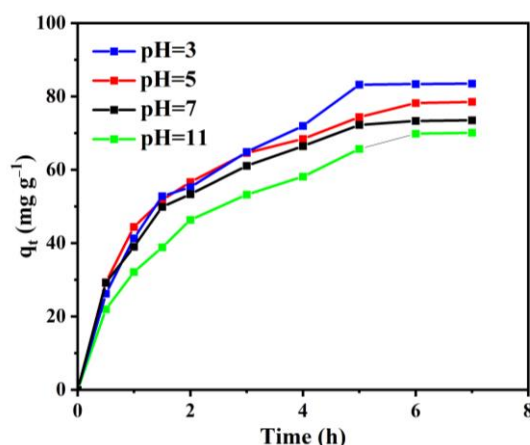


**Figure 6.** Effect of solution pH on uptake capacity of activated carbon at initial RB concentration of  $100 \text{ mg L}^{-1}$  and  $T=50^\circ\text{C}$ .

To investigate the mechanism of the adsorption process, the kinetic data and the related kinetic parameters were simulated by employing both the typical pseudo-first-order and pseudo-second-order kinetic models (Table 2) (Equations (3) and (4)). The parameters obtained from the adsorption of RB onto activated carbon based on the pseudo-second-order kinetic model match our experimental results well, with the highest  $R^2$ .

**Table 2.** Parameters of kinetic models for the adsorption of RB onto the activated carbon (Equations (3) and (4)).

Kinetic Models Parameters	Pseudo-First Order				Pseudo-Second Order		
	$Q_{e,exp} \text{ (mg g}^{-1}\text{)}$	$Q_{e,cal} \text{ (mg g}^{-1}\text{)}$	$K_1 \text{ (min}^{-1}\text{)}$	$R^2$	$Q_{e,cal} \text{ (mg g}^{-1}\text{)}$	$K_2 \text{ (mg min}^{-1}\text{)}$	$R^2$
$50^\circ\text{C}$	80.5	60.3	0.0083	0.974	88.0	$1.7 \times 10^{-4}$	0.997
$35^\circ\text{C}$	44.9	36.6	0.0065	0.998	51.0	$2.2 \times 10^{-4}$	0.994
$20^\circ\text{C}$	33.1	22.2	0.0061	0.984	34.5	$4.9 \times 10^{-4}$	0.998
pH = 5	70.1	64.1	0.0081	0.956	81.2	$1.3 \times 10^{-4}$	0.990
pH = 7	83.5	66.7	0.0073	0.984	94.6	$9.8 \times 10^{-5}$	0.991
pH = 11	73.5	54.6	0.0086	0.993	82.6	$1.7 \times 10^{-4}$	0.994

From the XPS results, there are certain surface functional groups on the as-prepared activated carbon, including the carboxyl and hydroxyl groups. These surface functional groups could dissociate and then be negatively charged [35], thus becoming active sites.

The interaction between the negatively charged functional groups in the activated carbon and the positively charged functional groups in RB enhances the adsorption capacity of the activated carbon. Therefore, the adsorption capacity of the adsorbent is significantly affected by the solution pH. In the acidic solution, the amount of  $\text{H}^+$  will compete with RB molecules for the adsorption sites of the activated carbon [41]. Therefore, the uptake capacity of the activated carbon is decreased in the acidic solution. Moreover, the RB molecules will be transformed from cationic to zwitterionic by deprotonation of the carboxyl group if the value of pH is greater than 3.7 [13]. For this reason, the electrostatic interaction between the negatively charged activated carbon and the zwitterionic RB will be weakened, and then the uptake capacity of the activated carbon is decreased as the value of pH is increased. Due to the above two reasons, the adsorption capacity of the activated carbon changed with pH, as shown in Figure 6.

#### 4. Conclusions

In summary, we synthesized a low-cost activated carbon via physiochemical activation using waste coffee as a potential raw material.

The obtained activated carbon possesses a large surface area of about  $952.7 \text{ m}^2 \text{ g}^{-1}$  and can be used as an adsorbent to remove the RB from aqueous solution successfully. The maximum uptake capacity was achieved under the following appropriate conditions: an initial concentration of  $100 \text{ mg L}^{-1}$ , a temperature of  $50^\circ\text{C}$  and a pH value of 7. The enhanced adsorption properties of the activated carbon can be attributed to its unique porous carbon structure, especially for the negatively charged surface functional groups, which can promote strong electrostatic attraction with positively charged functional groups in RB. This study demonstrates that waste-coffee-derived activated carbon could be used as an alternative low-cost adsorbent to commercial activated carbon for the removal of various toxic dyes from aqueous solution.

**Author Contributions:** Conceptualization, D.Z.; methodology, D.Z.; software, H.-M.C.; validation, H.-M.C., W.-M.L. and D.Z.; formal analysis, H.-M.C. and D.Z.; investigation, H.-M.C.; resources, W.-M.L.; data curation, H.-M.C. and D.Z.; writing—original draft preparation, H.-M.C.; writing—review and editing, D.Z.; visualization, H.-M.C.; supervision, W.-M.L. and D.Z.; project administration, D.Z.; funding acquisition, W.-M.L. and D.Z. All authors have read and agreed to the published version of the manuscript.

**Funding:** This research was funded by Scientific and Technological Innovation Foundation of Shunde Innovation School, USTB (BK21BE010), Foshan Science and Technology Innovation Project (no.2018IT100363) and Foshan Talents Special Foundation (BKBS202003). And The APC was funded by Foshan Talents Special Foundation (BKBS202003).

**Institutional Review Board Statement:** Not applicable.

**Informed Consent Statement:** Not applicable.

**Data Availability Statement:** Not applicable.

**Conflicts of Interest:** The authors declare no conflict of interest.

## References

1. Gagrani, A.; Zhou, J.; Tsuzuki, T. Solvent free mechanochemical synthesis of  $\text{MnO}_2$  for the efficient degradation of Rhodamine-B. *Ceram. Int.* **2018**, *44*, 4694–4698. [[CrossRef](#)]
2. Blanchard, R.; Mekonnen, T.H. Synchronous pyrolysis and activation of poly (ethylene terephthalate) for the generation of activated carbon for dye contaminated wastewater treatment. *J. Environ. Chem. Eng.* **2022**, *10*, 108810. [[CrossRef](#)]
3. Baloo, L.; Isa, M.H.; Sapari, N.B.; Jagaba, A.H.; Wei, L.J.; Yavari, S.; Razali, R.; Vasu, R. Adsorptive removal of methylene blue and acid orange 10 dyes from aqueous solutions using oil palm wastes-derived activated carbons. *Alex. Eng. J.* **2021**, *60*, 5611–5629. [[CrossRef](#)]
4. Jagaba, A.H.; Kutty, S.R.M.; Baloo, L.; Hayder, G.; Birniwa, A.H.; Taha, A.T.B.; Mnzool, M.; Lawal, M.I. Waste derived biocomposite for simultaneous biosorption of organic matter and nutrients from green straw biorefinery effluent in continuous mode activated sludge systems. *Processes* **2022**, *10*, 2262. [[CrossRef](#)]
5. Lee, L.Z.; Zainia, M.A.A. One-step  $\text{ZnCl}_2/\text{FeCl}_3$  composites preparation of magnetic activated carbon for effective adsorption of rhodamine B dye. *Toxin Rev.* **2022**, *41*, 64–81. [[CrossRef](#)]
6. Sayed, M.; Pal, H. Supramolecularly assisted modulations in chromophoric properties and their possible applications: An overview. *J. Mater. Chem. C* **2016**, *4*, 2685–2706. [[CrossRef](#)]
7. Yusaf, A.; Usman, M.; Mansha, A.; Saeed, M.; Ahmad, M.; Siddiq, M. Micellar-enhanced ultrafiltration (MEUF) for removal of rhodamine B (RhB) from aqueous system. *J. Dispers. Sci. Technol.* **2022**, *43*, 336–348. [[CrossRef](#)]
8. Alakhras, F.; Ouachtak, H.; Alhajri, E.; Rehman, R.; Al-Mazaidh, G.; Anastopoulos, I.; Lima, E.C. Adsorptive removal of cationic rhodamine B dye from aqueous solutions using chitosan-derived schiff base. *Sep. Sci. Technol.* **2022**, *57*, 542–554. [[CrossRef](#)]
9. Steplin, P.S.S.; Ganesh, K.A.; Sarala, L.; Rajaram, R.; Sathiyam, A.; Princy, M.J.; Sharmila, L.I. Photocatalytic degradation of rhodamine B using zinc oxide activated charcoal polyaniline nanocomposite and its survival assessment using aquatic animal model. *ACS Sustain. Chem. Eng.* **2017**, *6*, 258–267. [[CrossRef](#)]
10. Bar, N.; Chowdhury, P. A brief review on advances in rhodamine B based chromic materials and their prospects. *ACS Appl. Electron. Mater.* **2022**, *4*, 3749–3771. [[CrossRef](#)]
11. Cheng, Y.Y.; Tsai, T.H. Pharmacokinetics and biodistribution of the illegal food colorant rhodamine B in rats. *J. Agric. Food Chem.* **2017**, *65*, 1078–1085. [[CrossRef](#)] [[PubMed](#)]
12. Peng, M.; Kaczmarek, A.M.; Hecke, K.V. Ratiometric thermometers based on rhodamine B and fluorescein dye-incorporated (nano) cyclodextrin metal-organic frameworks. *ACS Appl. Mater. Interfaces* **2022**, *14*, 14367–14379. [[CrossRef](#)] [[PubMed](#)]

13. Jakimińska, A.; Pawlicki, M.; Macyk, W. Photocatalytic transformation of rhodamine B to rhodamine-110—The mechanism revisited. *J. Photochem. Photobiol. A* **2022**, *433*, 114176. [[CrossRef](#)]
14. Baldisserrri, C.; Ortelli, S.; Blosi, M.; Costa, A.L. Pilot-plant study for the photocatalytic/electrochemical degradation of rhodamine B. *J. Environ. Chem. Eng.* **2018**, *6*, 1794–1804. [[CrossRef](#)]
15. Yazdani, E.B.; Mehrizad, A. Sonochemical preparation and photocatalytic application of Ag-ZnS-MWCNTs composite for the degradation of rhodamine B under visible light: Experimental design and kinetics modelling. *J. Mol. Liq.* **2018**, *255*, 102–112. [[CrossRef](#)]
16. Zhou, X.; Jia, K.; He, X.; Wei, S.; Wang, P.; Liu, X. Microemulsion self-assembling of novel amphiphilic block co-polyarylene ether nitriles and photosensitizer ZnPc towards hybrid superparticles for photocatalytic degradation of rhodamine B. *Mater. Chem. Phys.* **2018**, *207*, 212–220. [[CrossRef](#)]
17. Wang, M.; Han, J.; Guo, P.; Sun, M.; Zhang, Y.; Tong, Z.; You, M.; Lv, C. Hydrothermal synthesis of B-doped Bi<sub>2</sub>MoO<sub>6</sub> and its high photocatalytic performance for the degradation of Rhodamine B. *J. Phys. Chem. Solids* **2018**, *113*, 86–93. [[CrossRef](#)]
18. Zhang, Y.; Zhou, J.; Cai, W.; Zhou, J.; Li, Z. Enhanced photocatalytic performance and degradation pathway of rhodamine B over hierarchical double-shelled zinc nickel oxide hollow sphere heterojunction. *Appl. Surf. Sci.* **2018**, *430*, 549–560. [[CrossRef](#)]
19. Yilmaz, E.; Soylak, M. Use of vegetable oil in supported liquid membrane for the transport of Rhodamine B, A novel and simple deep eutectic solvent based liquid phase microextraction method for rhodamine B in cosmetic products and water samples prior to its spectrophotometric determination. *Spectrochim. Acta Part A* **2018**, *202*, 81–86.
20. Jinisha, R.; Gandhimathi, R.; Ramesh, S.T.; Nidheesh, P.V.; Velmathi, S. Removal of rhodamine B dye from aqueous solution by electro-fenton process using iron-doped mesoporous silica as a heterogeneous catalyst. *Chemosphere* **2018**, *200*, 446–454. [[CrossRef](#)]
21. Araújo, D.; Sáez, C.; Martínez-Huitle, C.A.; Cañizares, P.; Rodrigo, M.A. Influence of mediated processes on the removal of rhodamine with conductive-diamond electrochemical oxidation. *Appl. Catal. B* **2015**, *166–167*, 454–459. [[CrossRef](#)]
22. Saravanana, S.; Carolin, C.F.; Kumar, P.S.; Chitra, B.; Rangasamy, G. Biodegradation of textile dye rhodamine-B by *brevundimonas diminuta* and screening of their breakdown metabolites. *Chemosphere* **2022**, *308*, 136266. [[CrossRef](#)] [[PubMed](#)]
23. Nazir, M.A.; Najam, T.; Bashir, M.S.; Javed, M.S.; Bashir, M.A.; Imran, M.; Azhar, U.; Shah, S.S.A.; ur Rehman, A. Kinetics, isothermal and mechanistic insight into the adsorption of eosin yellow and malachite green from water via tri-metallic layered double hydroxide nanosheets. *Korean J. Chem. Eng.* **2022**, *39*, 216–226. [[CrossRef](#)]
24. Nazira, M.A.; Khana, N.A.; Cheng, C.; Shah, S.S.A.; Najam, T.; Arshadf, M.; Shariff, A.; Akhtare, S.; ur Rehmana, A. Surface induced growth of ZIF-67 at Co-layered double hydroxide: Removal of methylene blue and methyl orange from water. *Appl. Clay Sci.* **2020**, *190*, 105564. [[CrossRef](#)]
25. Liu, J.; Liu, X.; Sun, Y.; Sun, C.; Liu, H.; Stevens, L.A.; Li, K.; Snape, C.E. High density and super ultra-microporous-activated carbon macrospheres with high volumetric capacity for CO<sub>2</sub> capture. *Adv. Sustain. Syst.* **2018**, *2*, 1700115. [[CrossRef](#)]
26. Valkila, J. Do fair trade pricing policies reduce inequalities in coffee production and trade. *Dev. Policy Rev.* **2014**, *32*, 475–493. [[CrossRef](#)]
27. Hua, H.J.; Liu, J.Y.; Xu, Z.H.; Zhang, L.Y.; Cheng, B.; Hoc, W. Hierarchical porous Ni/Co-LDH hollow dodecahedron with excellent adsorption property for Congo red and Cr(VI) ions. *Appl. Surf. Sci.* **2019**, *478*, 981. [[CrossRef](#)]
28. Guo, Y.; Zhao, J.; Zhang, H.; Yang, S.; Qi, J.; Wang, Z.; Xu, H. Use of rice husk-based porous carbon for adsorption of rhodamine B from aqueous solutions. *Dye. Pigm.* **2005**, *66*, 123–128. [[CrossRef](#)]
29. Sattar, M.; Hayeeye, F.; Chinpa, W.; Sirichote, O. Preparation and characterization of poly (lactic acid)/activated carbon composite bead via phase inversion method and its use as adsorbent for rhodamine B in aqueous solution. *J. Environ. Chem. Eng.* **2017**, *5*, 3780–3791. [[CrossRef](#)]
30. Cheng, Z.-L.; Li, Y.-X.; Liu, Z. Fabrication of graphene oxide/silicalite-1 composites with hierarchical porous structure and investigation on their adsorption performance for rhodamine B. *J. Ind. Eng. Chem.* **2017**, *55*, 234–243. [[CrossRef](#)]
31. Guo, Z.; Zhang, J.; Liu, H. Ultra-high rhodamine B adsorption capacities from an aqueous solution by activated carbon derived from *Phragmites australis* doped with organic acid by phosphoric acid activation. *RSC Adv.* **2016**, *6*, 40818–40827. [[CrossRef](#)]
32. Xie, Q.; Bao, R.; Zheng, A.; Zhang, Y.; Wu, S.; Xie, C.; Zhao, P. Sustainable low-cost green electrodes with high volumetric capacitance for aqueous symmetric supercapacitors with high energy density. *ACS Sustain. Chem. Eng.* **2016**, *4*, 1422–1430. [[CrossRef](#)]
33. Espinosa, J.C.; Navalon, S.; Alvaro, M.; Dhakshinamoorthy, A.; Garcia, H. Reduction of C=C double bonds by hydrazine using active carbons as metal-free catalysts. *ACS Sustain. Chem. Eng.* **2018**, *6*, 5607–5614. [[CrossRef](#)]
34. Preethi, M.; Viswanathan, C.; Ponpandian, N. A metal-free, dual catalyst for the removal of rhodamine B using novel carbon quantum dots from muskmelon peel under sunlight and ultrasonication: A green way to clean the environment. *J. Photochem. Photobiol. A* **2022**, *426*, 113765. [[CrossRef](#)]
35. Eftekhari, S.; Habibi-Yangjeh, A.; Sohrabnezhad, S. Application of AlMCM-41 for competitive adsorption of methylene blue and rhodamine B: Thermodynamic and kinetic studies. *J. Hazard. Mater.* **2010**, *178*, 349–355. [[CrossRef](#)]
36. Gupta, V.K. Equilibrium and thermodynamic studies on the adsorption of the dye rhodamine-B onto mustard cake and activated carbon. *J. Chem. Eng. Data* **2015**, *55*, 5225–5229. [[CrossRef](#)]
37. Yun, Y.S.; Park, M.H.; Hong, S.J.; Lee, M.E.; Park, Y.W.; Jin, H.J. Najafpour removal of rhodamine B from aqueous solution using palm shell-based activated carbon: Adsorption and kinetic studies. *J. Chem. Eng. Data* **2010**, *55*, 5777–5785.

38. Rodriguez, A.; Garcia, J.; Ovejero, G.; Mestanza, M. Adsorption of anionic and cationic dyes on activated carbon from aqueous solutions: Equilibrium and kinetics. *J. Hazard. Mater.* **2009**, *172*, 1311–1320. [[CrossRef](#)]
39. Nazir, M.A.; Najam, T.; Shahzad, K.; Wattoo, M.A.; Hussain, T.; Tufail, M.K.; Shah, S.S.A.; ur Rehman, A. Heterointerface engineering of water stable ZIF-8@ZIF-67: Adsorption of rhodamine B from water. *Surf. Interfaces* **2022**, *34*, 102324. [[CrossRef](#)]
40. Saleh, T.A.; Ali, I. Synthesis of polyamide grafted carbon microspheres for removal of rhodamine B dye and heavy metals. *J. Environ. Chem. Eng.* **2018**, *6*, 5361–5368. [[CrossRef](#)]
41. Shi, W.N.; Fang, W.-X.; Wang, J.-C.; Qiao, X.; Wang, B.B.; Guo, X.W. pH-controlled mechanism of photocatalytic RhB degradation over g-C<sub>3</sub>N<sub>4</sub> under sunlight irradiation. *Photochem. Photobiol. Sci.* **2021**, *20*, 303–313. [[CrossRef](#)] [[PubMed](#)]